Environmental Science & Technology

pubs.acs.org/est

Article

Global Mercury Assimilation by Vegetation

Jun Zhou and Daniel Obrist*

Cite This: *Environ. Sci. Technol.* 2021, 55, 14245−14257

Read Online

ACCESS | Metrics & More | Article Recommendations | Supporting Information

ABSTRACT: Assimilation of mercury (Hg) by vegetation represents one of the largest global environmental Hg mass fluxes. We estimate Hg assimilation by vegetation globally via a bottom-up scaling approach using tissue Hg concentrations synthesized from a comprehensive database multiplied by respective annual biomass production (NPP). As global annual NPP is close to annual vegetation die-off, Hg mass associated with global NPP approximates the transfer of Hg from plants to soils, which represents an estimate of vegetation-mediated atmospheric deposition. Annual vegetation assimilation of Hg from combined atmospheric and soil uptake is estimated at 3062 ± 607 Mg yr^{-1}, which is composed of 2491 ± 551 Mg yr^{-1} from aboveground tissue uptake and 571 ± 253 Mg yr^{-1} from root uptake. Assimilation of atmospheric Hg amounts to 2422 ± 483 Mg yr^{-1} when considering aboveground tissues only. Atmospheric assimilation increases to 2705 ± 504 Mg yr^{-1} when considering that root Hg may be partially derived from prior foliar uptake and transported internally to roots. Estimated atmospheric Hg assimilation by vegetation is 54−137% larger than the current model and litterfall estimates, largely because of the inclusion of lichens, mosses, and woody tissues in deposition and all global biomes. Belowground, about 50% of root Hg was taken up from soils with currently unknown ecological and biogeochemical consequences.

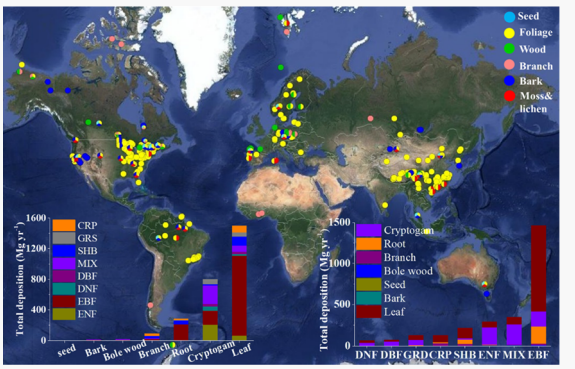

KEYWORDS: *plant tissues, biome, elemental Hg deposition, oxidized Hg deposition, geogenic Hg assimilation*

1. INTRODUCTION

Anthropogenic mercury (Hg) emissions have elevated atmospheric Hg concentrations and deposition to ecosystems several-fold since the Industrial Revolution.[1] The terrestrial environment is an important component of the global Hg cycle and is estimated to receive 3600 Mg of atmospheric Hg deposition annually, equivalent to about half of total annual Hg emissions to the atmosphere from anthropogenic and natural sources combined (with the remainder depositing to global oceans).[2] Atmospheric Hg deposition includes wet deposition via precipitation and snow and dry deposition, which includes the removal of particulate Hg and sorption and uptake of gaseous Hg to Earth's surfaces.[3,4] Multiple lines of evidence show that dry deposition of gaseous elemental Hg (Hg(0)) via vegetation uptake, however, is the dominant Hg source to terrestrial environments whereby atmospheric Hg(0) is taken up by vegetation tissues and subsequently transferred and deposited to soils when tissues are shed (litterfall), plants die off (biomass turnover), and leaf surfaces are washed off (i.e., throughfall).[5,6] Global data analyses estimate global Hg deposition by litterfall in the range of 1020−1230 Mg yr^{-1}, and global throughfall deposition is considered in a similar range.[5,7−9] Global model simulations estimate total atmospheric deposition via vegetation in the range of 1310−1570 Mg yr^{-1} [10] and 1400 Mg yr^{-1},[11] constituting one of the largest global sinks of atmospheric Hg, e.g., exceeding global terrestrial wet deposition of 730−1070 Mg yr^{-1}.[10]

Global estimates of Hg deposition associated with vegetation are commonly constrained using forest litterfall measurements, yet the use of litterfall alone to estimate vegetation Hg deposition may significantly underestimate deposition.[12] A study along a glacier-to-forest succession suggested that litterfall deposition underestimated total vegetation Hg deposition by 65% because it failed to account for assimilation of Hg(0) by mosses, inputs from woody tissues, and throughfall deposition,[6] and contributions by woody tissues and whole tree turnover have been estimated to enhance deposition by 60% compared to leaf litter deposition alone in forests.[13] A recent study showed that atmospheric Hg(0) deposition in a deciduous forest is three times greater than litterfall mercury deposition measurements.[14] In addition, a study that summarized Hg concentrations in mosses estimated Hg assimilation via mosses to globally account for 630 ± 320 Mg yr^{-1},[6] which is about half of deposition by litterfall.[5,7−9] Finally, global litterfall Hg estimates commonly focus on forests but neglect vegetation Hg uptake in other biomes such

Received: June 1, 2021
Revised: September 23, 2021
Accepted: September 24, 2021
Published: October 7, 2021

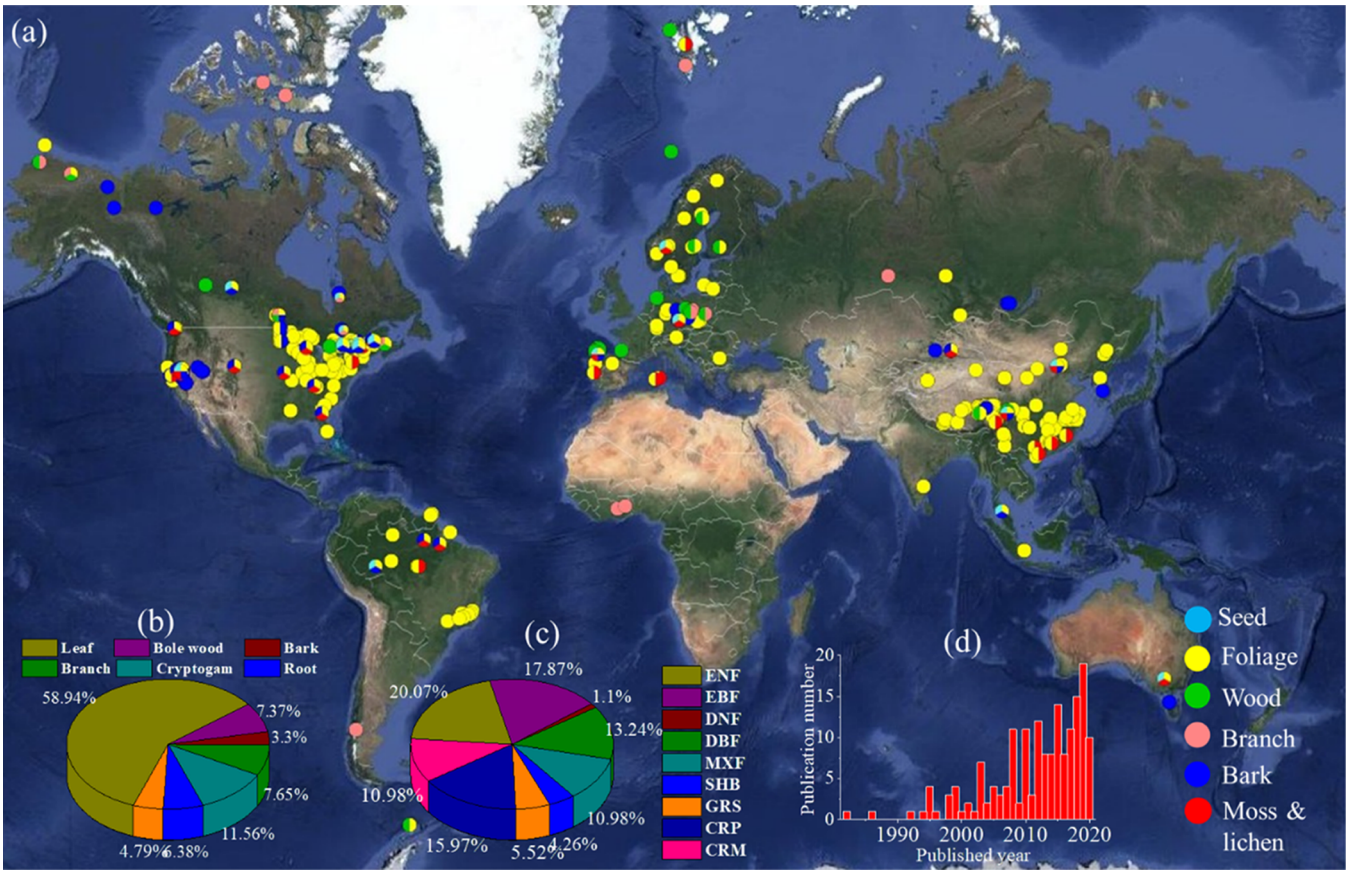

Figure 1. (a) Global spatial distribution of Hg measurement in plant tissues and functional groups (a), sample sizes of plant tissues and functional groups (b) and biomes, and number of publications per year (d).

as cropland, grassland, and shrubland, which globally account for 27% of the terrestrial land surface.

Here, we perform a bottom-up estimate of Hg assimilation by global vegetation considering all major global biomes and tissues. We comprehensively analyzed available Hg data in vegetation using a global database to constrain Hg concentrations in all major plant functional groups and tissue types across global biomes. The database includes Hg concentrations from 198 studies, spans from 1980 and 2021, and includes 1918 measurement points based on estimated 60 000 samples analyzed across 494 locations in the world. We combine statistical distributions of Hg concentration data from the database with the annual biomass production (net primary productivity: NPP) for all tissue categories and major biomes to quantify the total global Hg assimilation associated with annually produced tissues across global biomes. As global NPP is close to global vegetation die-off,[15] Hg assimilation associated with global NPP also represents an estimate of the transfer of Hg from plants to soils during biomass die-off and in the case of an atmospheric Hg source, an estimate of vegetation-mediated atmospheric deposition. We hence also separate vegetation Hg assimilation based on the respective source origins of Hg based on the recent stable Hg isotope source attribution studies, specifically to separate atmospheric and geogenic sources to estimate global atmospheric deposition, internal ecosystems (e.g., soil−plant Hg) recycling, and transport between aboveground to belowground tissues.

2. MATERIALS AND METHODS

2.1. Collection of Vegetation Hg Data in a Global Database. We developed a comprehensive database from peer-reviewed studies that reported Hg concentrations from different biome types, tissues, and functional groups, which were published between 1980 and 2021. The database was originally published in Zhou et al.[10] and has been expanded by an additional 35 published studies for this analysis. The updated database is published in the Supporting Information. We did not separate or weigh data based on sampling years as no clear temporal trends in tissue Hg concentrations were observed among the 40 years of published studies (Figure S1). The lack of such time trends may be due to temporal biases in the availability of data for different tissue types, species, and locations along with a low number of time replicates for individual tissues and species. The database represents 494 sites across the world (Figure 1a,d) and was structured to separate Hg concentrations from different tissues (leaf, needle, bulk litterfall, woody tissues including bole wood, bark, branch, and root); plant functional groups (lichen, moss, and vascular plants including grassland plant, crop, and tree) (Figure 1b); and biome types (deciduous broadleaf forest (DBF), deciduous needleleaf forest (DNF), evergreen broadleaf forest (EBF), evergreen needleleaf forest (ENF), mixed forest (MIX), grassland (GRS), shrubland (SHB), and cropland (CRP)) (Figure 1c). Each data point collected was a reported Hg concentration in a published study, whereby most data points consist of many individual measurements so that we estimate that the data set represented about 60,000 individual

https://doi.org/10.1021/acs.est.1c03530
Environ. Sci. Technol. 2021, 55, 14245−14257

Table 1. Summary of Hg Concentration and Global Estimated Hg Assimilation Separated by Vegetation Tissues and Biomes

ecosystem	tissue	mean Hg concentration (ng g^{-1})	median Hg concentration (ng g^{-1})	NPP (Pg biomass yr^{-1})	Hg assimilation (Mg yr^{-1}) mean	95% confidence intervals	median
evergreen needleleaf forest	leaf	27 ± 14	25	2.46	65 ± 33	61−70	61
	bole wood	2 ± 1	2	1.2	3 ± 2	3−3	3
	branch	16 ± 7	19	0.38	6 ± 3	5−8	7
	bark	17 ± 7	10	0.366	6 ± 2	5−8	7
	cryptogam	109 ± 74	87	1.87	206 ± 141	181−232	164
	root	38 ± 22	28	1.38	7 ± 4	5−9	7
	total				293 ± 145		249
evergreen broadleaf forest	leaf	53 ± 24	51	19.6	1045 ± 471	988−1102	999
	bole wood	2 ± 1	2	5.12	9 ± 5	6−12	10
	branch	12 ± 11	14	1.66	20 ± 18	12−28	23
	bark	4 ± 3	2	0.94	4 ± 3	0.6−2	2
	cryptogam	87 ± 45	85	2.11	183 ± 95	148−217	179
	root	38 ± 31	31	7.7	292 ± 236	204−380	235
	total				1553 ± 536		1448
deciduous needle forest	leaf	49 ± 16	51	0.5	20 ± 7	19−22	20
	bole wood	3 ± 0	3	0.28	0.5 ± 0.3	0.4−0.6	0.5
	branch	19 ± 2	19	0.076	0.8 ± 0.4	0.7−1	0.9
	bark	19 ± 2	19	0.026	0.2 ± 0.3	0.2−0.3	0.2
	cryptogam	109 ± 74	87	0.49	53 ± 36	47−60	42
	root	0	0	0.26	1 ± 0.7	0.9−1	1
	total				76 ± 37		65
deciduous broadleaf forest	leaf	41 ± 15	40	0.7	29 ± 11	27−30	28
	bole wood	2 ± 1	1	0.34	0.6 ± 0.4	0.5−0.8	0.6
	branch	12 ± 5	12	0.112	1 ± 0.6	1−1	1
	bark	9 ± 6	6	0.032	0.3 ± 0.2	0.3−0.4	0.2
	cryptogam	76 ± 27	74	0.33	36 ± 24	31−40	29
	root	7 ±	7	0.26	0.3 ± 0.2	0.2−0.4	0.3
	total				67 ± 26		59
mixed broadleaf and needleleaf forest	leaf	25 ± 15	21	3.36	83 ± 50	76−89	70
	bole wood	3 ± 1	2	2.48	7 ± 3	5−9	5
	branch	5 ± 2	6	0.72	8 ± 4	6−9	8
	bark	13 ± 5	14	0.68	7 ± 4	1−2	5
	cryptogam	109 ± 74	87	2.22	241 ± 164	212−271	192
	root	7 ± 3	6	1.38	1± 0.7	1−1	1
	total				347 ± 172		282
shrubland	leaf	19 ± 17	11	12.74	119 ± 111	79−159	68
	branch	6 ± 7	2	5	32 ± 37	13−52	12
	cryptogam	109 ± 74	87	0.16	17 ± 12	15−20	14
	root	19 ± 26	3	14.02	71 ± 40	55−87	70
	total				239 ± 124		164
grassland	leaf	20 ± 10	20	2.82	58 ± 29	51−64	56
	cryptogam	43 ± 23	34	1.31	62 ± 36	52−71	52
	root	41 ± 31	30	2.22	91 ± 52	75−107	78
	total				212 ± 68		186
cropland	leaf	28 ± 16	27	2.7	82 ± 47	72−93	81
	branch	21 ± 13	19	3.46	71 ± 45	59−84	66
	seed	9 ± 10	5	3.72	15 ± 5	14−16	15
	root	41 ± 21	38	1.08	108 ± 63	89−127	93
	total				276 ± 90	99	255
the global	leaf	34 ± 21	31	44.88	1501 ± 491		1383
	bole wood	2 ± 1	2	9.42	20 ± 6		19
	branch	15 ± 11	13	11.41	139 ± 61		118
	bark	13 ± 7	13	2.04	18 ± 5		14
	cryptogam	83 ± 65	66	8.49	798 ± 243		672
	seed	9 ± 10	5	3.72	15 ± 5		15
	root	29 ± 29	18	28.30	571 ± 253		485
	total			108.27	3062 ± 607		2707

https://doi.org/10.1021/acs.est.1c03530
Environ. Sci. Technol. 2021, 55, 14245−14257

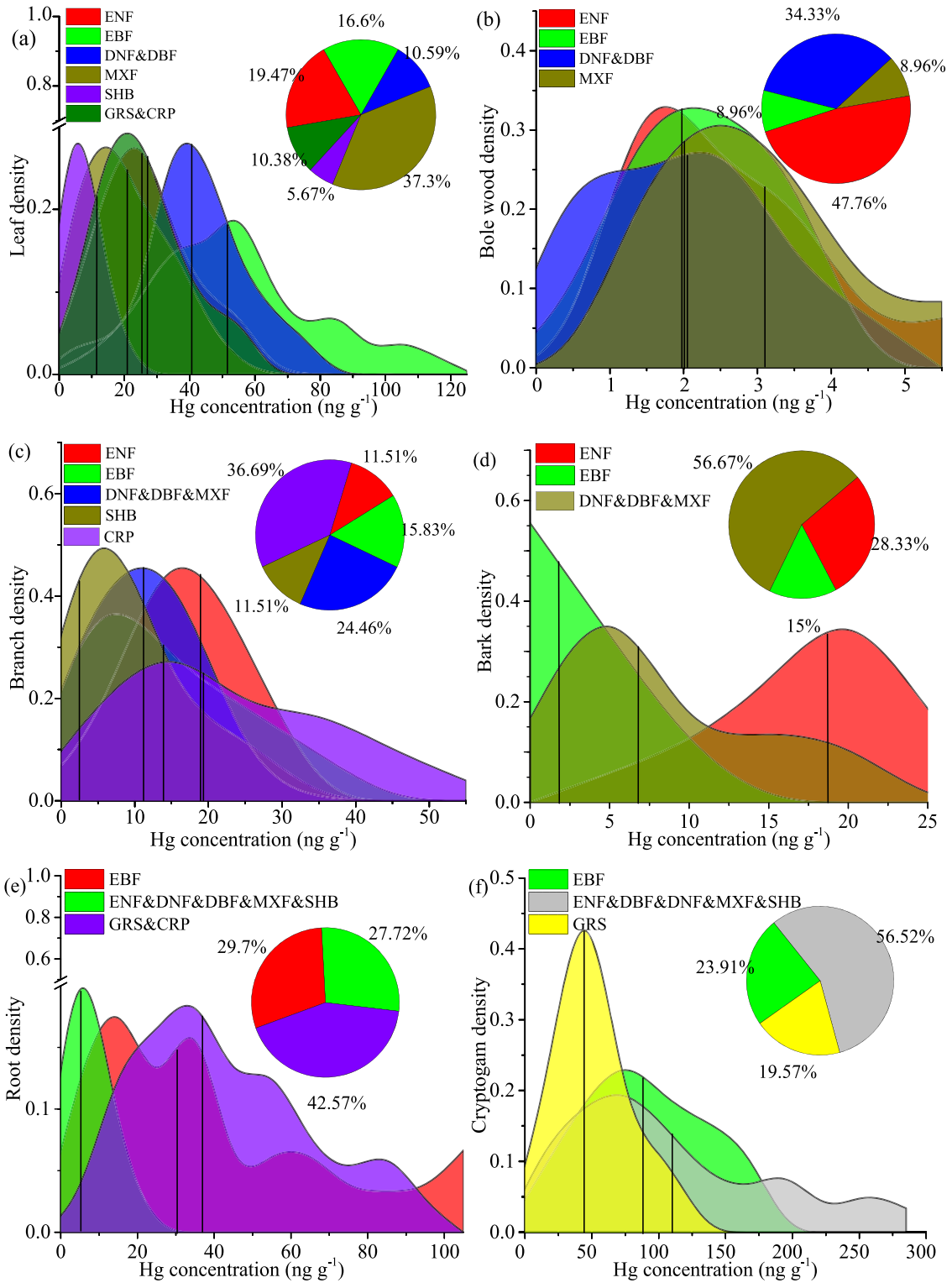

Figure 2. Distribution density of the measured Hg concentration in foliage (a), bole wood (b), branch (c), bark (d), root (e), and cryptogam (f) samples collected globally. Vertical lines represent mean values for each tissue category. For some tissue categories, several biomes were combined based on geographic or ecological similarities to obtain sufficient sample numbers to characterize distributions.

plant tissue Hg measurements. Data are from a total of 198 studies from background locations. We eliminated all data points from areas we considered impacted by specific point source pollution sources and hence excluded Hg-enriched areas such as industrial, mining, and urban sites from our data set. The reasons for this are Hg-enriched data are likely overproportionally represented in the database, are extremely difficult to scale up quantitatively to global scales, and likely represent only a small percentage of the global surface area (e.g., <1% of soils in the United States were found to be Hg-enriched).[16] Hence, our approach to exclude Hg-enriched data may provide a lower-bound estimate of global Hg assimilation

https://doi.org/10.1021/acs.est.1c03530
Environ. Sci. Technol. 2021, 55, 14245−14257

by vegetation. Further, plants of Hg hyperaccumulators are also not included in the manuscript because they represent a negligible amount of global NPP. We performed statistical outlier analyses for each class of observations (i.e., tissue for each biome type) based on an interquartile rule, which removed 5% of all data (total 1828 remaining data points). The resulting background data set on Hg plant concentrations involve 1918 individual data points, including 225 for cryptogams (lichens and mosses), 1492 for foliage and litterfall, 147 for roots, 73 for bark, 149 for branch, 112 for seed, and 149 for wood. Overall, a high number of data points (1828 measurement points in 494 locations) allow representativeness of data for most tissue types, although some tissue categories show smaller data availability and hence larger uncertainties. For example, data for bole wood, branch, bark, moss, and lichen were limited to 134, 139, 77, 90, and 145 data points, respectively, and combined accounted for less than 27% of all data.

2.2. Global Annual Vegetation Biomass of Terrestrial Biomes. To estimate global annual Hg assimilation by vegetation, estimates of mean and median Hg concentration and uncertainty ranges were multiplied with the amount of annually produced biomass (i.e., net primary productivity: NPP) for each tissue and all biomes. We did not include or propagate error estimates associated with NPP data as their respective errors (1−2%)[17] generally are much smaller than the uncertainty range of tissue Hg concentrations (see below). NPP for vascular vegetation was obtained from Cleveland et al.[18] and Zhao and Running,[17] providing NPP for the nine major global biomes. Because no Hg concentration data were available for savannas and woody savannas, we combined these two biomes with the biome shrubland. In addition, crops contribute about 10% of global NPP, and we used cropland NPP (5.42 Pg biomass yr^{-1}) from Monfreda et al.[19] to estimate Hg assimilation in cropland (CRP). NPP estimates by Cleveland et al.[18] and Zhao and Running[17] used moderate resolution imaging spectroradiometer data, which did not specifically account for cryptogamic NPP (i.e., by mosses and lichens). To estimate Hg assimilation by cryptogams, we added NPP data from Elbert et al.[20] along with the respective Hg concentration data for each biome. Cryptogam NPP was reported for the category "tropical forests" and "extratropical forests" and "steppe, desert, and tundra", which we distributed into the following biomes based on their respective areal distributions (Tables 1 and S1): tropical cryptogam was considered as biome EBF; extratropical cryptogams were distributed to ENF, DBF, DNF, MIX, and SHB; and steppe, desert, and tundra cryptogams were attributed to the biome GRS. To convert NPP estimates in units of mass carbon (Pg C m^{-2} yr^{-1}) to biomass NPP, we used a carbon content of 45% C for cryptogam dry biomass and 50% C for all other tissue biomasses.[21] When combining NPP estimates from these various sources (i.e., nine global biomes: 88.82 Pg biomass yr^{-1},[17,18] cryptogams: 7.64 Pg biomass yr^{-1},[20] and crops: 10.96 Pg biomass yr^{-1}),[19] their sum (108.27 Pg biomass yr^{-1}) is similar to the estimated global terrestrial NPP of 109.2 Pg biomass yr^{-1} for the time period 2000−2009 calculated by the dynamic land ecosystem model.[22]

We allocated NPP to different tissues (root, stem, foliage) following the global data set of Cleveland et al.,[18] which separates NPP for leaves, stems, and roots across nine major global biomes (DBF, deciduous broadleaf forest; DNF, deciduous needleleaf forest; EBF, evergreen broadleaf forest; ENF, evergreen needleleaf forest; GRS, grassland; MIX, mixed forest; SHB, closed shrublands; SVN, savannas; and WSV, woody savannas). As Cleveland et al.[18] did not separate stem biomass further into bole wood, bark, and branch, we used a second data set by Chen et al.,[23] which includes 196 study sites (12 EBF sites, 117 ENF sites, 51 DBF sites, 1 DNF sites, and 15 MXF sites) to separate stem NPP into branches and stemwood (i.e., combined bole wood and bark). Finally, we use several papers from forest biomes to further differentiate stemwood into bark and bole wood (DBF,[24] EBF,[25] ENF,[26] and MIX).[26] We calculated assimilation by seeds only for crop biomes where seed production accounts for a substantial amount of NPP.[27−29] Further information about biomass and NPP estimates for all tissues and biomes is reported in Table S1 of the Supporting Information. Because both global NPP and standing biomass are relatively stable over decadal time scales (see Section 3),[15,22] we assume near-steady-state conditions where annual NPP equals approximates annual plant die-off of biomass so that Hg assimilated by annual NPP is also an estimate for annual turnover, which in case of atmospheric uptake of Hg directly represents an atmospheric deposition estimate (see Section 3 for details and limitations of this approach).

2.3. Estimation of Global Hg Assimilation by Vegetation. We calculate summary statistics of Hg concentrations in the database for all biomes and tissues (except for cryptogams in cropland where no data were available). Annual Hg assimilation (MA, Mg yr^{-1}) by vegetation tissues (T) in each biome type (B) is calculated using the following formula

$$MA_T = \sum_{i=1}^{n} C_i \times BM_i \times X\% \quad (1)$$

$$MA_B = \sum_{T=1}^{n} MA_T \quad (2)$$

where C_i ($\mu g\ kg^{-1}$) and BM_i ($g\ m^{-2}$) are the Hg concentrations and annual biomass production of respective vegetation tissues plus cryptogams, respectively, and n is the tissue number of tissues in each biome. When sample sizes for tissue Hg concentrations were too small in a biome, we combined data from climatically or ecologically similar biomes to calculate Hg concentration distribution statistics, for example, combining leaf Hg concentrations of DNF and DBF, as well as GRS and CRP (Figure 2). Resulting data on Hg concentration distributions shown in Figure 2 for various biomes were all normally distributed except data on foliage Hg in mixed forests ($p = 0.03$). For uncertainty analyses and error propagation, we calculate mean Hg tissue concentrations and standard deviations (Table 1) and in addition provide median values and interquartile ranges (IQRs). Cryptogam Hg concentrations in the database are largely represented by lichens and mosses and lack data for other growth forms (see Section 3).

The term X% in eq 1 represents percentages of Hg derived from atmospheric Hg(0) and Hg(II) sources, as well as from geogenic uptake (i.e., derived from geologic substrates), based on stable Hg isotope studies by Wang et al.[6] and Zhou et al.[10] in forests and shrubland, by Mao et al.[30] in grassland, and by Yin et al.[31] in cropland tissues. Current source attributions to differentiate atmospheric Hg(0) and Hg(II) and geogenic sources in tissues rely on a large number of studies for foliage, which reveal consistent patterns of dominant atmospheric Hg(0) sources (summary by Zhou et al.[10]). However, stable

https://doi.org/10.1021/acs.est.1c03530
Environ. Sci. Technol. 2021, 55, 14245−14257

isotope data for many other tissues are limited in the number of biomes and species (e.g., Wang et al.[6] for other forest tissues; Yin et al.[31] for rice tissues) so that source attribution may be biased by biomes or geographically.[10,32] We estimate uncertainties in Hg sources based on reported source uncertainties from stable Hg isotope data and further consider the current uncertainties associated with this approach in Section 3.

2.4. Statistical Analysis. We used SPSS software (SPSS Inc. 16) to calculate summary statistics across all tissue types, biome types, and geographic domains. All tissue Hg concentrations for biomes (with the exception of one) were normally distributed. We use mean values and standard deviation to estimate uncertainties and accumulate uncertainties of cumulative sums of tissues and biomes using square roots of standard deviations. In addition, we also provide median values and IQR in tables. Differences in Hg concentrations among groups of data were tested using two-way analysis of variance (ANOVAs) and post hoc Tukey HSD tests ($p = 05$). Linear correlations were analyzed by Spearman correlation coefficient (r) tests.

3. RESULTS AND DISCUSSION

3.1. Hg Concentrations across Vegetation Tissues and Biomes in the Global Database. Mean Hg concentrations and IQR across functional groups and vegetation tissues significantly vary in the following order: lichen (137 ± 75 $\mu g\ kg^{-1}$) > moss (58 ± 31 $\mu g\ kg^{-1}$) > litterfall (45 ± 15 $\mu g\ kg^{-1}$) > root (31 ± 27 $\mu g\ kg^{-1}$) > foliage (23 ± 15 $\mu g\ kg^{-1}$) > branch (15 ± 11 $\mu g\ kg^{-1}$) > bark (13 ± 7 $\mu g\ kg^{-1}$) > grass (9 ± 8 $\mu g\ kg^{-1}$) > bole wood (2 ± 1 $\mu g\ kg^{-1}$) (Figure S2). Cryptogams (mosses and lichens) show the highest Hg concentrations (83 ± 65 $\mu g\ kg^{-1}$) of all tissues. The natural stable isotope abundance shows that 76% and 86% of ground and tree moss Hg are derived from atmospheric Hg(0) uptake, respectively, with the remainder from atmospheric Hg(II) uptake.[6] In our global database, mosses and lichens show the highest mean Hg concentrations in tropical forests (evergreen broadleaf forest), followed by extratropical forests, tundra (SHB), and steppe (GRS) (Figure 2f).

In vascular plants, we combined green leaves and needles together with litterfall samples for the tissue category "foliage" because published litterfall Hg concentrations largely consist of recently fallen leaf and needle tissues.[33,34] Hg concentration of foliage includes 1071 data points, and Hg concentrations ranged from 2 to 114 $\mu g\ kg^{-1}$, with an overall mean (±SD) of 34 ± 21 $\mu g\ kg^{-1}$ and a median of 31 $\mu g\ kg^{-1}$ (Figure 2a). Hg concentrations in foliage generally show the highest concentrations of any tissue in vascular plants (Figure S3). In our global database, the highest foliage Hg concentrations are observed in the evergreen broadleaf forest biome, followed by deciduous needleleaf forest and deciduous broadleaf forest, which were significantly higher than that in evergreen needleleaf forest and mixed forest (Figure S3a), similar to patterns of previous global litterfall Hg analysis studies.[5] Many stable isotope signature and atmosphere-foliage exchange studies show that an estimated 88% (IQR: 79−100%) of Hg in vegetation originates from the uptake of atmospheric Hg(0).[10,35]

Bole wood Hg concentrations (2 ± 1 $\mu g\ kg^{-1}$) are by far the lowest of any tissues (Figures 2b and S3b). In our database, Hg concentrations in bole wood are highest in deciduous needleleaf forests, followed by evergreen needleleaf forests, mixed forests, evergreen broadleaf forests, and deciduous broadleaf forests. While uptake pathways of bole Hg are not completely clear, they likely include a combination of root uptake, foliage uptake, and transfer from the bark.[10] Recently, a number of studies suggested that Hg accumulation by bole wood is largely from foliar uptake and subsequent translocation via phloem, while translocation from roots and bark is negligible.[36−46] A recent isotope study estimated that atmospheric Hg(0) and Hg(II) account for 84 ± 25% (rang: 83−88%) and 4 ± 9% (rang: 3−11%) of total Hg in bole wood, respectively.[6] The mean Hg concentration in bark (4 ± 3 to 19 ± 2 $\mu g\ kg^{-1}$ across different biomes) is similar to those of branches (7 ± 3 to 41 ± 31 $\mu g\ kg^{-1}$) (Tables 1 and S2). Hg concentrations in branches and bark show substantial variability across and within biomes (Figures 2c,d and S3c,d), similar to high variability also reported across and within trees of the same forest.[47] Hg in bark and branches is considered to largely originate from atmospheric uptake via passive surface adsorption,[42,48−51] and atmospheric Hg(0) and Hg(II) reportedly accounted for 81 ± 25 and 5 ± 9% in bark and 84 ± 25 and 4 ± 9% in branches.

Root concentrations in our database show a wide range of Hg concentrations from 7 ± 3 to 41 ± 31 $\mu g\ kg^{-1}$ across various biomes (Figures 2e and S3e). Uptake mechanisms and pathways of Hg by roots are poorly known[10] but have largely been attributed to soil uptake.[38,52,53] A recent isotope study using rice and sawgrass roots supported that most root Hg was derived from soils and foliage-to-root transport accounted for only 10.3−12.4%.[30,31] Another study, in contrast, recently showed that between 44 and 83% of Hg in tree roots was derived from atmospheric Hg(0)[6] (see Section 3).

3.2. Global Annual Assimilation and Turnover of Hg by Vegetation. We here estimate the total global Hg assimilation by vegetation using a bottom-up scaling approach using tissue-specific Hg concentrations multiplied by the respective annual NPP of tissue categories across all global biomes. These calculations provide direct estimates of annual Hg assimilation by global biomass, separated by biomes and tissue types, and provide an estimate of the atmospheric uptake when sources derive from atmospheric uptake. Note that as long as annual NPP is similar to annual vegetation die-off, the calculated Hg assimilation also represents the transfer of vegetation Hg to soils and litter. Globally, biomass pools are quite stable (e.g., changing about 0.78 Pg biomass yr^{-1} between 1998 and 2002 or <0.1‰ of the vegetation pool size)[15] so that there is a near-equilibrium between annually produced global biomass (NPP) and annual die-off. A caveat to this is that regionally, tropical areas experience biomass losses due to deforestation (−0.42 Pg biomass yr^{-1}), which on a global scale is largely compensated by increasing biomass pools in boreal and temperate mixed forests (+0.36 Pg biomass yr^{-1}) driven by regrowth of abandoned farmland and afforestation programs. Our approach hence somewhat overestimates Hg transfer from vegetation to soils in temperate and boreal forests (where NPP > die-off) and underestimates transfer in tropical forests (NPP < die-off), although the errors are likely small (<0.1%).

The mean global Hg assimilation by vegetation is calculated at 3062 ± 607 Mg yr^{-1}, with a median value of 2707 Mg yr^{-1} (Table 2). Note that if we used site means to estimate Hg assimilation by vegetation instead of unweighted distribution statistics, the annual global Hg assimilation value would be 23% larger (3779 ± 773 Mg yr^{-1}) (Table S3). The largest

https://doi.org/10.1021/acs.est.1c03530
Environ. Sci. Technol. 2021, 55, 14245−14257

Table 2. Global Hg Assimilation by Vegetation (Mg yr^{-1}) and Source Origins Separated by Tissues and Biomes

			average source percentage (%, range)[a]			assimilation by source (range), in Mg Hg yr^{-1}			
ecosystem	tissue	Hg assimilation (mean ± std) (Mg Hg yr^{-1})	Hg (0)	Hg (II)	geogenic	Hg (0)	Hg (II)	atmospheric (Hg (0) + Hg (II))	geogenic
evergreen needleleaf forest	leaf	65 ± 33	88 (79−100)	12 (14−24)	0	57 ± 29 (51−65)	8 ± 4 (0−14)	65 ± 29 (51−79)	0
	bole wood	3 ± 2	84 (83−88)	4 (4−6)	12 (6−14)	3 ± 2 (2−3)	0.1 ± 0.1 (0.1−0.2)	3 ± 2 (2−3)	0.4 ± 0.2 (0.2−0.4)
	branch	6 ± 3	84 (79−87)	4 (5−6)	12 (10−18)	5 ± 3 (5−5)	0.2 ± 0.1 (0.2−0.4)	5 ± 3 (5−5)	0.7 ± 0.4 (0.6−1)
	bark	6 ± 2	81 (62−92)	5 (3−10)	14 (5−29)	5 ± 5 (4−6)	0.3 ± 0.1 (0.18−0.6)	5 ± 2 (4−6)	0.8 ± 0.3 (0.3−2)
	cryptogam	206 ± 141	81 (95−118)	19 (14−24)	0	167 ± 114 (157−177)	39 ± 27 (29−49)	206 ± 117 (186−226)	0
	root	7 ± 4	59 (44−83)	11 (4−28)	30 (12−42)	4 ± 2 (3−6)	0.8 ± 0.4 (0.3−2)	5 ± 2 (3−8)	2 ± 1 (0.8−3)
	total	293 ± 145				241 ± 118 (222−261)	48 ± 27 (30−66)	289 ± 121 (252−327)	4 ± 1 (2−6)
evergreen broadleaf forest	leaf	1045 ± 471	88 (79−100)	12 (14−24)	0	920 ± 414 (826−1045)	125 ± 57 (0−219)	1045 ± 418 (826−1264)	0
	bole wood	9 ± 5	84 (83−88)	4 (4−6)	12 (6−14)	8 ± 4 (7−8)	0.4 ± 0.2 (0.4−0.5)	8 ± 4 (7−9)	1 ± 0.6 (0.5−1)
	branch	20 ± 18	84 (79−87)	4 (5−6)	12 (10−18)	17 ± 15 (16−17)	0.8 ± 0.7 (0.6−1)	18 ± 15 (17−18)	2 ± 2 (2−4)
	bark	4 ± 3	81 (62−92)	5 (3−10)	14 (5−29)	3 ± 2 (3−4)	0.2 ± 0.2 (0.1−0.4)	3 ± 2 (3−4)	0.6 ± 0.4 (0.2−1)
	cryptogam	183 ± 95	81 (76−86)	19 (14−24)	0	148 ± 77 (139−157)	35 ± 18 (26−44)	183 ± 79 (165−201)	0
	root	292 ± 236	59 (44−83)	11 (4−28)	30 (12−42)	172 ± 139 (128−242)	32 ± 26 (12−82)	204 ± 142 (140−324)	88 ± 71 (35−123)
	total	1553 ± 536				1268 ± 444 (1119−1474)	194 ± 65 (38−347)	1461 ± 449 (1157−1821)	92 ± 71 (38−129)
deciduous needle forest	leaf	20 ± 7	88 (79−100)	12 (14−24)	0	18 ± 6 (16−20)	2 ± 0.8 (0−4)	20 ± 6 (16−24)	0
	bole wood	0.5 ± 0.3	84 (83−88)	4 (4−6)	12 (6−14)	0.4 ± 0.3 (0.4−0.4)	0.02 ± 0.01 (0.02−0.03)	0.4 ± 0.3 (0.4−0.4)	0.06 ± 0.04 (0.03−0.07)
	branch	0.8 ± 0.4	84 (79−87)	4 (5−6)	12 (10−18)	0.7 ± 0.3 (0.6−0.7)	0.03 ± 0.02 (0.02−0.05)	0.7 ± 0.3 (0.6−0.8)	0.1 ± 0.05 (0.08−0.1)
	bark	0.2 ± 0.3	81 (62−92)	5 (3−10)	14 (5−29)	0.2 ± 0.2 (0.1−0.2)	0.01 ± 0.02 (0.01−0.02)	0.17 ± 0.24 (0.11−0.22)	0.03 ± 0.04 (0.01−0.06)
	cryptogam	53 ± 36	81 (76−86)	19 (14−24)	0	43 ± 29 (40−46)	10 ± 7 (7−13)	53 ± 30 (47−59)	0
	root	1 ± 0.7	59 (44−83)	11 (4−28)	30 (12−42)	0.7 ± 0.4 (0.5−1)	0.1 ± 0.1 (0−0.3)	0.8 ± 0.4 (0.5−1)	0.4 ± 0.2 (0.1−0.5)
	total	76 ± 37				62 ± 30 (58−68)	13 ± 7 (8−17)	75 ± 31 (66−85)	0.5 ± 0.2 (0.3−0.8)
deciduous broadleaf forest	leaf	29 ± 11	88 (79−100)	12 (14−24)	0	26 ± 10 (23−29)	3 ± 1 (0−6)	29 ± 10 (23−35)	0
	bole wood	0.6 ± 0.4	84 (83−88)	4 (4−6)	12 (6−14)	0.5 ± 0.3 (0.5−0.5)	0.02 ± 0.02 (0.02−0.04)	0.5 ± 0.3 (0.5−0.5)	0.1 ± 0 (0−0.1)
	branch	1 ± 0.6	84 (79−87)	4 (5−6)	12 (10−18)	1 ± 0.5 (0.9−1)	0.05 ± 0.02 (0.04−0.07)	1 ± 0.5 (0.9−1)	0.1 ± 0.1 (0.1−0.2)
	bark	0.3 ± 0.2	81 (62−92)	5 (3−10)	14 (5−29)	0.2 ± 0.2 (0.2−0.3)	0.02 ± 0.01 (0.01−0.03)	0.3 ± 0.2 (0.2−0.3)	0.04 ± 0.03 (0.01−0.1)
	cryptogam	36 ± 24	81 (76−86)	19 (14−24)	0	29 ± 19 (27−31)	7 ± 5 (5−9)	36 ± 20 (32−40)	0
	root	0.3 ± 0.2	59 (44−83)	11 (4−28)	30 (12−42)	0.2 ± 0.1 (0.1−0.2)	0.03 ± 0.02 (0.01−0.08)	0.2 ± 0.1 (0.1−0.3)	0.1 ± 0.1 (0−0.1)

https://doi.org/10.1021/acs.est.1c03530
Environ. Sci. Technol. 2021, 55, 14245−14257

Table 2. continued

ecosystem	tissue	Hg assimilation (mean ± std) (Mg Hg yr^{-1})	average source percentage (%, range)[a]			assimilation by source (range), in Mg Hg yr^{-1}			
			Hg (0)	Hg (II)	geogenic	Hg (0)	Hg (II)	atmospheric (Hg (0) + Hg (II))	geogenic
	total	67 ± 26				57 ± 22 (52−62)	10 ± 5 (5−15)	67 ± 22 (57−77)	0.3 ± 0.1 (0.2−0.5)
mixed broadleaf and needleleaf forest	leaf	83 ± 50	88 (79−100)	12 (14−24)	0	73 ± 44 (66−83)	10 ± 6 (0−17)	83 ± 44 (66−100)	0
	bole wood	7 ± 3	84 (83−88)	4 (4−6)	12 (6−14)	6 ± 3 (6−6)	0.3 ± 0.1 (0.3−0.4)	6 ± 3 (6−6)	0.8 ± 0.4 (0.4−1)
	branch	8 ± 4	84 (79−87)	4 (5−6)	12 (10−18)	7 ± 3 (6−7)	0.3 ± 0.2 (0.2−0.5)	7 ± 3 (6−8)	1 ± 0.5 (0.8−1)
	bark	7 ± 4	81 (62−92)	5 (3−10)	14 (5−29)	6 ± 3 (4−6)	0.4 ± 0.2 (0.2−0.7)	6 ± 3 (5−7)	1 ± 0.6 (0.4−2)
	cryptogam	241 ± 164	81 (76−86)	19 (14−24)	0	195 ± 133 (183−207)	46 ± 31 (34−58)	241 ± 136 (217−265)	0
	root	1± 0.7	59 (44−83)	11 (4−28)	30 (12−42)	0.7 ± 0.4 (0.5−1)	0.1 ± 0.1 (0.05−0.3)	0.8 ± 0.4 (0.6−1)	0.4 ± 0.2 (0.1−0.5)
	total	347 ± 172				287 ± 140 (266−311)	57 ± 32 (35−77)	344 ± 144 (301−388)	3 ± 0.8 (2−5)
shrubland	leaf	119 ± 111	88 (79−100)	12 (14−24)	0	105 ± 98 (94−119)	14 ± 13 (0−25)	119 ± 99 (94−144)	0 ± 0 (0−0)
	branch	32 ± 37	84 (83−88)	4 (5−6)	12 (10−18)	27 ± 31 (27−28)	1 ± 2 (1−2)	28 ± 31 (28−30)	4 ± 4 (3−6)
	cryptogam	17 ± 12	81 (76−86)	19 (14−24)	0	14 ± 10 (13−15)	3 ± 2 (2−4)	17 ± 10 (15−19)	0 ± 0 (0−0)
	root	71 ± 40	59 (44−83)	11 (4−28)	30 (12−42)	42 ± 24 (31−59)	8 ± 4 (3−20)	50 ± 24 (34−79)	21 ± 12 (9−30)
	total	239 ± 124				187 ± 106 (165−221)	27 ± 14 (6−51)	214 ± 107 (171−272)	25 ± 13 (12−36)
grassland	leaf	58 ± 29	93 (87−95)	0	7 (5−13)	54 ± 27 (50−55)	0	54 ± 27 (50−55)	4 ± 2 (3−8)
	cryptogam	62 ± 36	81 (76−86)	19 (14−24)	0	50 ± 29 (47−53)	12 ± 7 (9−15)	62 ± 30 (56−68)	0
	root	91 ± 52	11 (10−12)	0	89 (88−90)	10 ± 6 (9−11)	0	10 ± 6 (9−11)	80 ± 46 (79−81)
	total	212 ± 68				114 ± 40 (107−120)	12 ± 7 (9−15)	126 ± 41 (116−135)	85 ± 46 (82−89)
cropland	leaf	82 ± 47	100 (62−100)	0	0 (0−38)	82 ± 47 (51−82)	0	82 ± 47 (51−82)	0 ± 0 (0−31)
	branch	71 ± 45	44 (35−52)	0	56 (48−65)	31 ± 20 (25−37)	0	31 ± 20 (25−37)	40 ± 25 (34−46)
	seed	15 ± 5	22 (21−23)	0	78 (77−80)	3 ± 1 (3−3)	0	3 ± 1 (3−3)	12 ± 4 (12−12)
	root	108 ± 63	11 (10−12)	0	89 (88−90)	12 ± 7 (11−13)	0	12 ± 7 (11−13)	96 ± 55 (95−97)
	total	276 ± 90				129 ± 51 (90−136)	0	129 ± 51 (90−136)	148 ± 61 (140−186)
the global	leaf	1501 ± 491	93−100 (62−100)	0 (0−24)	(0−7)	1333 ± 433 (1176−1498)	163 ± 59 (0−286)	1497 ± 437 (1176−1784)	4 ± 2 (3−39)
	bole wood	20 ± 6	84 (83−88)	4 (0−6)	12 (6−14)	17 ± 5 (17−18)	0.8 ± 0.3 (0.8−1)	18 ± 5 (18−19)	2 ± 0.8 (1−3)
	branch	139 ± 61	44−84 (35−88)	24 (0−6)	12−56 (10−65)	88 ± 40 (80−97)	3 ± 2 (2−4)	91 ± 40 (82−101)	48 ± 26 (41−58)
	bark	18 ± 5	81 (62−92)	5 (0−10)	14 (5−29)	14 ± 4 (11−16)	0.9 ± 0.3 (0.5−2)	15 ± 4 (12−18)	3 ± 0.8 (0.9−5)
	cryptogam	798 ± 243	81 (76−86)	19 (0−24)	0	646 ± 197 (606−686)	152 ± 46 (112−192)	798 ± 202 (718−878)	0

https://doi.org/10.1021/acs.est.1c03530
Environ. Sci. Technol. 2021, 55, 14245−14257

Table 2. continued

ecosystem	tissue	Hg assimilation (mean ± std) (Mg Hg yr^{-1})	average source percentage (%, range)[a]			assimilation by source (range), in Mg Hg yr^{-1}			
			Hg (0)	Hg (II)	geogenic	Hg (0)	Hg (II)	atmospheric (Hg (0) + Hg (II))	geogenic
	seed	15 ± 5	22 (21−23)	0	78 (77−80)	3 ± 1 (3−3)	0	3 ± 1 (3−3)	12 ± 4 (12−12)
	root	571 ± 253	11−59 (10−83)	11 (0−28)	30−89 (12−90)	242 ± 142 (184−334)	41 ± 26 (15−104)	283 ± 144 (199−438)	288 ± 102 (219−335)
	total	3062 ± 607				2345 ± 498 (1731−2242)	360 ± 79 (130−589)	2705 ± 504 (1861−2831)	357 ± 105 (276−452)

[a]The percentages of plant assimilation Hg source in forest and shrubland are from Wang et al.[6] and Zhou et al.,[10] and grassland and cropland are from Mao et al.[30] and Yin et al.[31] Numbers in parentheses represent the uncertainty range of mean estimates based on uncertainties in source contributions.

contributions to global Hg assimilation stem from foliage uptake (49%), which accounts for a mean of 1501 ± 491 Mg yr^{-1} and a median of 1383 Mg yr^{-1} (Table 2 and Figure S4). Cryptogamic tissues (i.e., mosses and lichens) show a global mean Hg assimilation of 798 ± 243 Mg yr^{-1} and a median of 672 Mg yr^{-1}, accounting for about 26% of the total Hg assimilation by vegetation (Table 1 and Figure S4). Hence, despite accounting for only 7% of global NPP (Table S1), cryptogams contribute considerably to global Hg vegetation assimilation due to tissue Hg concentrations that are two to six times higher than those of foliage (Figure 3 and Table 1). Hg assimilation in roots is estimated at 571 ± 253 Mg yr^{-1} (mean) and 485 Mg yr^{-1} (median) and accounts for 19% of total global Hg assimilation by vegetation.

Total Hg assimilation by woody aboveground tissues (branch, bole wood, and bark) amounts to a mean of 177 ± 61 Mg yr^{-1} and a median of 151 Mg yr^{-1}. Of woody tissues, Hg assimilation is dominated by branches (average: 139 ± 61 [median: 118] Mg yr^{-1}, which includes forest branches, shrub stems, and crop stems), followed by bole wood (20 ± 6 [19] Mg yr^{-1}) and bark (18 ± 5 [14] Mg yr^{-1}) (Table 1 and Figure S4), accounting for 5%, 0.7%, and 0.6% of total Hg vegetation assimilation, respectively. The combined contributions of all woody tissues to Hg assimilation (6.3%) are much lower than their contributions to biomass NPP (e.g., 14% for bole wood) due to generally low Hg concentrations of woody tissues. Finally, Hg uptake by seeds of cropland biomes results in a global Hg assimilation of 15 ± 5 Mg yr^{-1} (mean) and 15 Mg yr^{-1} (median), accounting for 0.5% of global Hg vegetation assimilation.

3.3. Global Atmospheric Hg(0) and Hg(II) and Geogenic Hg Assimilation by Vegetation. Source origins of Hg assimilated by vegetation are important as they determine atmosphere-to-soil transfer (in case of an atmospheric source) versus intrasystem Hg cycling (e.g., soil−vegetation−soil in case of soil Hg sources). We hence separated Hg assimilation into respective Hg sources (i.e., atmospheric versus soil uptake) and different atmospheric Hg species (i.e., Hg(0) versus Hg(II)), acknowledging that while source attribution studies are reliable for foliage and based on about a dozen different studies (review by Zhou et al.[10]), sources are more uncertain for other tissues and based on a few studies only resulting in considerable uncertainties. Based on available studies, we estimate that atmospheric Hg(0) contributes 88% (79−100%) in foliage, 84% (83−88%) in bole wood, 84% (79−87%) in branches, 81% (62−92%) in bark, 59% (44−83%) in roots, and 81% (76−86%) in cryptogams. Source percentages in grassland and cropland are from Mao et al.[30] and Yin et al.[31] Please note that rice is the only crop we are aware of with stable isotope source information, but we find that experimental and tracer studies indicate similar patterns of dominant atmospheric sources of Hg in aboveground tissues of crops (e.g., maize, wheat, and oilseed rape).[54,55] Using these source estimates shows that of the calculated total global Hg vegetation assimilation of 3062 ± 607 Mg yr^{-1}, the largest part (2345 ± 498 Mg yr^{-1} or 77%) is derived from atmospheric Hg(0) uptake, while atmospheric Hg(II) uptake contributes to about 360 ± 79 Mg yr^{-1} (12%) and geogenic Hg uptake accounts for about 357 ± 105 Mg yr^{-1} (12%) (Table 2). Note that uncertainties in source attributions currently are large as indicated also by a large uncertainty range (estimated in parentheses in Table 2). Uncertainties are particularly high in roots where one available isotope study

https://doi.org/10.1021/acs.est.1c03530
Environ. Sci. Technol. 2021, 55, 14245−14257

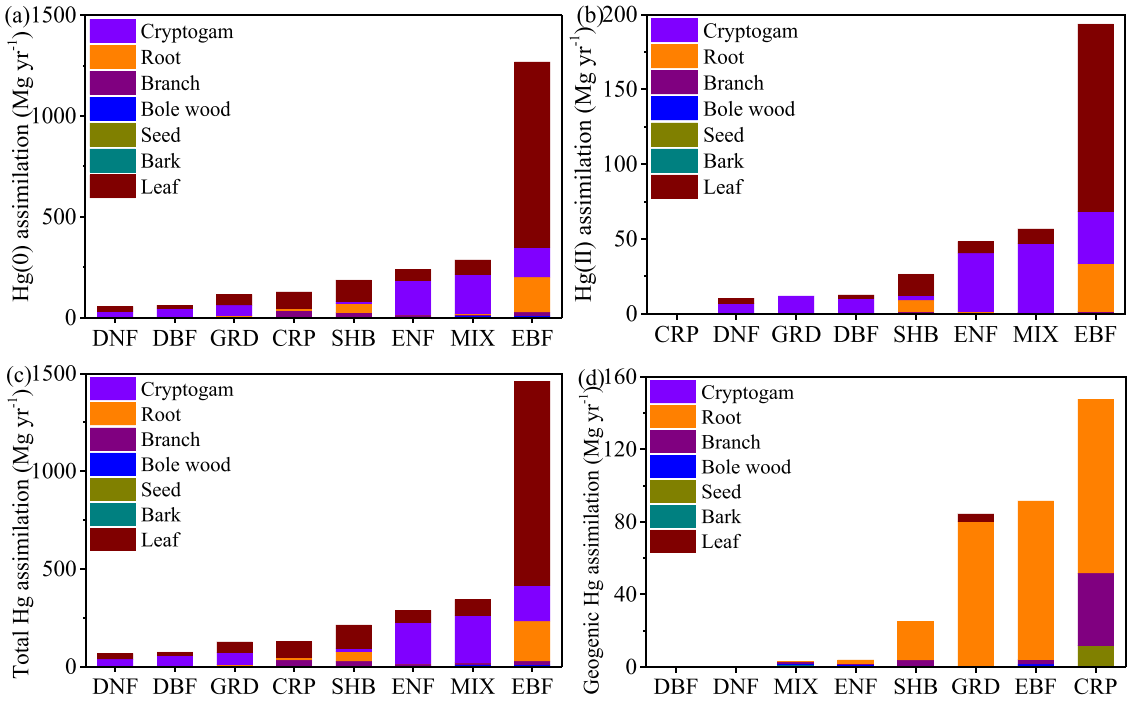

Figure 3. Hg assimilation by vegetation of atmospheric Hg(0) (a), atmospheric Hg(II) (b), total atmospheric Hg (Hg(0) and Hg(II)) (c), and geogenic Hg (d) separated by biomes and excluding root Hg assimilation.

shows atmospheric Hg(0) sources between 44 and 83% in tree roots.[6]

For aboveground tissues, we calculate a global Hg assimilation of 2113 ± 477 Mg yr^{-1} from atmospheric Hg(0), 320 ± 75 Mg yr^{-1} from atmospheric Hg(II), and 149 ± 53 Mg yr^{-1} from geogenic sources subsequently translocated to aboveground tissues (Tables S4 and 2). The combined atmospheric Hg assimilation by aboveground tissues is 2433 ± 483 Mg yr^{-1}, a pool that is subject to transfer to litter and soils when plant tissues die (i.e., deposition). The largest part of aboveground atmospheric Hg assimilation is attributable to foliage (62%, mean of 1497 ± 437 Mg yr^{-1}), followed by cryptogams (33%, 798 ± 202 Mg yr^{-1}) and branches (4%, 91 ± 40 Mg yr^{-1}) (Figure S4). Bole wood assimilation accounts for 1% (18 ± 5 Mg yr^{-1}) of aboveground Hg assimilation only. Hence, while aboveground woody tissues account for 124 ± 41 Mg yr^{-1} or 5% of total atmospheric Hg assimilation, the flux is driven largely by branches and bark with little contributions by bole wood.

Not surprisingly, root Hg assimilation accounts for the largest proportion of geogenic Hg assimilation (81% of the total geogenic uptake) and is estimated at 288 ± 102 Mg yr^{-1} (Figure S4d). This is followed by geogenic Hg assimilated in branches (14%), presumably after internal root-to-shoot transfer. Globally, we calculate that 19% of total geogenic Hg taken up by plants was translocated to aboveground tissues. These estimates are consistent with previous studies showing generally minor translocations of soil Hg to aboveground biomass.[6,38,56] The role of roots regarding atmospheric Hg sources merits further and careful consideration, however. For a long time, Hg in roots has largely been attributed to belowground uptake, but recent stable Hg isotope studies now have reported significant atmospheric Hg sources in tree roots, with a median estimate of 59% (range of 44−83%) of root Hg deriving from atmospheric Hg(0) and 11% (range of 4−28%) from atmospheric Hg(II).[6] Another study showed lower atmospheric contributions in roots of grassland and crop plants (total of 11%).[31] These studies hence suggest the possibility that a significant proportion of root Hg originally was assimilated from the atmosphere by foliage and subsequently translocated to belowground tissues. If indeed all root Hg with an atmospheric isotope signature originates from atmospheric Hg uptake, this would increase the total global atmospheric Hg assimilation by plants to 2705 ± 504 Mg yr^{-1}, an increase of 11% compared to considering aboveground tissues only (2433 ± 483 Mg yr^{-1}) (Table 2). Further studies are needed to confirm the ultimate sources of Hg in roots and internal shoot-to-root transport, in particular, given their potential to substantially enhance (+11%) atmospheric Hg uptake and deposition by vegetation. Possibly, roots may show more complex sources as reports have shown that smaller roots may show lower atmospheric Hg contributions than larger roots.[6,31]

Our estimates of vegetation-derived Hg assimilation, which results in deposition during plant tissue die-off, are substantially larger than previous estimates based on global litterfall data and global model simulations. Atmospheric Hg deposition via litterfall was estimated in the range of ∼1100−1300 Mg yr^{-1}.[5,7−9] A recent global model simulation using the GEM-MACH-Hg model[10] estimated the total terrestrial Hg deposition (wet + dry) of about 2800 Mg y^{-1}, whereby vegetation-derived Hg deposition was between 1310 and 1570 Mg yr^{-1}. That study also estimated that 90% of vegetation deposition derived from atmospheric Hg(0) (1180−1410 Mg yr^{-1}) and 10% from oxidized Hg(II) (130−160 Mg yr^{-1}). A GEOS-Chem model study estimated vegetation-derived Hg(0) deposition of 1400 Mg yr^{-1}.[1111] Our estimates of atmospheric Hg deposition by aboveground tissues only (Table S4) are 2113 ± 477 Mg yr^{-1} for Hg(0) and 320 ± 75 Mg yr^{-1} for Hg(II) deposition for a combined atmosphere-to-surface flux of 2433 ± 483 Mg yr^{-1}. Including root Hg with atmospheric signatures, atmospheric Hg assimilation would increase to

https://doi.org/10.1021/acs.est.1c03530
Environ. Sci. Technol. 2021, 55, 14245−14257

2345 ± 498 Mg yr^{-1} for Hg(0) and 361 ± 79 Mg yr^{-1} for Hg(II) for a combined flux of 2706 ± 504 Mg yr^{-1}.

Major reasons for higher plant Hg assimilation are that our study includes all global biomes (i.e., including forests, grassland, shrubland, and cropland) and considers Hg assimilation associated with more tissue categories (i.e., including woody tissues, roots, and cryptogams). Specifically, we recommend accounting for atmospheric assimilation by woody tissues (estimated at 124 ± 41 Mg yr^{-1}), by global crops (estimated at 129 ± 51 Mg yr^{-1}), and most importantly by cryptogams (estimated at 798 ± 202 Mg yr^{-1}; Table 1). When considering global Hg assimilation via foliar (leaves and needles) and litterfall only, our global Hg assimilation of 1497 ± 437 Mg yr^{-1} is closer to previous litterfall estimates (1100−1300 Mg yr^{-1},[5,7−9] based on litterfall Hg data across about 90 forest sites). Our results also estimate atmospheric Hg assimilation by cryptogams of 798 ± 202 Mg yr^{-1}, of which cryptogamic Hg assimilation in forests is 719 ± 240 Mg yr^{-1} and assimilation in shrubland and grasslands is 79 ± 38 Mg yr^{-1} (Table 1) and which combined is about 53% of atmospheric Hg assimilation by global foliage. These estimates are slightly higher than a recent study that estimated Hg assimilation by forest mosses of 630 ± 320 Mg yr^{-1},[6] and both studies hence suggest that assessing cryptogam Hg dynamics is important for global Hg assimilation and deposition. To further constrain this globally important flux, current uncertainties such as lack of Hg concentration data from many cryptogamic growth forms (e.g., biological soil and rock crusts, bryophyte, epiphytic, and epiphyllic crusts), more refined distribution of cryptogam NPP and Hg concentrations within biomes, and information on driving patterns for local and regional cryptogam distribution patterns need to be resolved. We further suggest to better constrain current uncertainties in root Hg concentrations and sources as roots may account for 283 ± 144 Mg yr^{-1} of atmospheric Hg taken up by foliage and translocated belowground each year.

In addition to die-off of plant tissues, throughfall Hg deposition is an additional vegetation-derived atmospheric deposition flux, and this flux is not included in our Hg assimilation estimates. To the best of our knowledge, throughfall deposition has only been quantified in forests and is estimated globally at about 1340 Mg yr^{-1},[57,58] accounting for 90, 75, and 143% of litterfall Hg deposition estimates in forests in China, Europe, and North America, respectively.[59] In throughfall, 34−82% of Hg may be derived from atmospheric Hg(0), while the rest is considered atmospheric Hg(II). Combined, total vegetation-derived Hg contributions (i.e., via plant turnover + throughfall) may hence be ∼4046 Mg yr^{-1} when considering atmospheric Hg assimilation transported to roots or ∼3773 Mg yr^{-1} without considering root transport. Both estimates imply a much higher turnover rate of the global atmospheric Hg pool (about 4800 Mg[60]), which on average may entirely cycle through the global vegetation pool about every 1.2−1.3 years.

3.4. Global Spatial Distribution of Atmospheric Hg Deposition by Vegetation. Although tissues show regional variability in Hg concentrations (in parts indeed related to atmospheric Hg exposures; see above), we find that global Hg assimilation is most strongly determined by respective regional and biome-specific biomass NPPs (Table S1). Ranking atmospheric Hg assimilation according to biomes (not including root transfer; Figure 3 and Table S4), we find evergreen broadleaf forests (EBFs), which are largely located in tropical areas, to show by far the highest atmospheric Hg assimilation of 1,461 ± 449 Mg yr^{-1} (1268 ± 444 and 194 ± 65 Mg yr^{-1} for atmospheric Hg(0) and Hg(II), respectively), accounting for 54% of the total global Hg deposition by vegetation. Biomes that contribute further to global atmospheric Hg assimilation, in order of their importance, are mixed forest (344 ± 144 Mg yr^{-1}), evergreen needleleaf forest (289 ± 121 Mg yr^{-1}), shrubland (214 ± 107 Mg yr^{-1}), cropland (129 ± 51 Mg yr^{-1}), grassland (127 ± 39 Mg yr^{-1}), deciduous needleleaf forest (75 ± 31 Mg yr^{-1}), and deciduous broadleaf forest (67 ± 22 Mg yr^{-1}) (Figure 3c). Note also that strong biases exist with respect to available Hg data across biomes (Figure 1c), and most results are available from evergreen needleleaf forest (20%), with a global surface area of 6.17 Mio km^2. Sample numbers for some other biomes are much smaller, for example, 6, 11, and 4% for grasslands, mixed forests, and shrublands, which represent large surface coverages of 11.15, 7.46, and 45.38 Mio km^2, respectively.[18] Global uncertainties could be reduced by the collection of Hg tissue data from savannas and woody savannas and from woody tissues and cryptogam tissues where data are generally scarce. In addition, the detailed description of sampling locations, protocols, and environmental exposures (atmosphere and soils) and consistent sampling protocols would help reduce Hg distribution patterns geographically and across biomes.

In Table S4, we calculate the annual atmospheric Hg assimilation per unit surface area (i.e., area-based deposition flux). Not considering potential atmospheric Hg transfer to roots, vegetation-derived deposition fluxes are in the following order, from highest to lowest: evergreen broadleaf forest > deciduous broadleaf forest > deciduous needleleaf forest ≈ evergreen needleleaf forest ≈ mixed broadleaf and needleleaf forest > grassland > cropland > shrubland. Our estimated area-based deposition fluxes by biomes are much higher than deposition rates based on global models.[6,10] For example, compared to a GEM-MACH-Hg model study, our data exceed modeled Hg assimilation fluxes by 435% in evergreen needleleaf forest, by 226% in deciduous broadleaf forest, and by 185% in deciduous needleleaf forest. Note, however, that vegetation Hg assimilation fluxes are not equal to ecosystem net Hg(0) exchange fluxes since they do not account for Hg(0) re-emission that occur from surfaces after deposition.[57,61] Further work is required to reconcile the current differences in bottom-up and top-down estimates of Hg assimilation by vegetation as they have important implications for global estimates of ecosystem Hg deposition loads and internal Hg cycling within ecosystems between soils and vegetation.

■ ASSOCIATED CONTENT

Supporting Information

The Supporting Information is available free of charge at https://pubs.acs.org/doi/10.1021/acs.est.1c03530.

Global NPP (in Pg biomass yr^{-1}) for all global biomes separated by tissue category and including cryptogams; summary of Hg assimilation (Mg yr^{-1}) by vegetation tissues in each biome; box plots of Hg concentrations for leaf and litterfall data as a function of the year of data published; and box charts for Hg concentrations in foliage, bole wood, branch, bark, root, and cryptogam for different global biomes (PDF)

https://doi.org/10.1021/acs.est.1c03530
Environ. Sci. Technol. 2021, 55, 14245−14257

Global vegetation mercury concentration database (XLSX)

AUTHOR INFORMATION

Corresponding Author

Daniel Obrist − *Department of Environmental, Earth, and Atmospheric Sciences, University of Massachusetts, Lowell, Massachusetts 01854, United States*; Phone: +1 978-934-3069; Email: daniel_obrist@uml.edu

Author

Jun Zhou − *Department of Environmental, Earth, and Atmospheric Sciences, University of Massachusetts, Lowell, Massachusetts 01854, United States*; orcid.org/0000-0001-9914-6808

Complete contact information is available at: https://pubs.acs.org/10.1021/acs.est.1c03530

Notes

The authors declare no competing financial interest.

ACKNOWLEDGMENTS

This work was supported by the U.S. National Science Foundation (AGS award # 1848212 and DEB award # 2027038).

REFERENCES

(1) Mason, R. P.; Fitzgerald, W. F.; Morel, F. M. The biogeochemical cycling of elemental mercury: anthropogenic influences. *Geochim. Cosmochim. Acta* **1994**, *58*, 3191−3198.

(2) Outridge, P. M.; Mason, R. P.; Wang, F.; Guerrero, S.; Heimburger-Boavida, L. E. Updated global and oceanic mercury budgets for the united nations global mercury assessment 2018. *Environ. Sci. Technol.* **2018**, *52*, 11466−11477.

(3) Zhang, L.; Wright, L. P.; Blanchard, P. A review of current knowledge concerning dry deposition of atmospheric mercury. *Atmos. Environ.* **2009**, *43*, 5853−5864.

(4) Zhou, J.; Wang, Z.; Zhang, X.; Driscoll, C. T. Measurement of the vertical distribution of gaseous elemental mercury concentration in soil pore air of subtropical and temperate forests. *Environ. Sci. Technol.* **2021**, *55*, 2132−2142.

(5) Wang, X.; Bao, Z. D.; Lin, C. J.; Yuan, W.; Feng, X. B. Assessment of global mercury deposition through litterfall. *Environ. Sci. Technol.* **2016**, *50*, 8548−8557.

(6) Wang, X.; Yuan, W.; Lin, C.-J.; Luo, J.; Wang, F.; Feng, X.; Fu, X.; Liu, C. Underestimated sink of atmospheric mercury in a deglaciated forest chronosequence. *Environ. Sci. Technol.* **2020**, *54*, 8083−8093.

(7) Fu, X.; Yang, X.; Lang, X.; Zhou, J.; Zhang, H.; Yu, B.; Yan, H.; Lin, C.-J.; Feng, X. Atmospheric wet and litterfall mercury deposition at urban and rural sites in China. *Atmos. Chem. Phys.* **2016**, *16*, 11547−11562.

(8) Wright, L. P.; Zhang, L.; Marsik, F. J. Overview of mercury dry deposition, litterfall, and throughfall studies. *Atmos. Chem. Phys.* **2016**, *16*, 13399−13416.

(9) Zhang, L.; Wu, Z.; Cheng, I.; Wright, L. P.; Olson, M. L.; Gay, D. A.; Risch, M. R.; Brooks, S.; Castro, M. S.; Conley, G. D.; Edgerton, E. S.; Holsen, T. M.; Luke, W.; Tordon, R.; Weiss-Penzias, P. The estimated six-year mercury dry deposition across North America. *Environ. Sci. Technol.* **2016**, *50*, 12864−12873.

(10) Zhou, J.; Obrist, D.; Dastoor, A.; Jiskra, M.; Ryjkov, A. Mercury uptake by vegetation and impact on global mercury cycling. *Nat. Rev. Earth Environ.* **2021**, *2*, 269−284.

(11) Song, S.; Selin, N. E.; Soerensen, A. L.; Angot, H.; Artz, R.; Brooks, S.; Brunke, E. G.; Conley, G.; Dommergue, A.; Ebinghaus, R.; Holsen, T. M.; Jaffe, D. A.; Kang, S.; Kelley, P.; Luke, W. T.; Magand, O.; Marumoto, K.; Pfaffhuber, K. A.; Ren, X.; Sheu, G. R.; Slemr, F.; Warneke, T.; Weigelt, A.; Weiss-Penzias, P.; Wip, D. C.; Zhang, Q. Top-down constraints on atmospheric mercury emissions and implications for global biogeochemical cycling. *Atmos. Chem. Phys.* **2015**, *15*, 7103−7125.

(12) Obrist, D.; Kirk, J. L.; Zhang, L.; Sunderland, E. M.; Jiskra, M.; Selin, N. E. A review of global environmental mercury processes in response to human and natural perturbations: Changes of emissions, climate, and land use. *Ambio* **2018**, *47*, 116−140.

(13) Obrist, D. Atmospheric mercury pollution due to losses of terrestrial carbon pools? *Biogeochemistry* **2007**, *85*, 119−123.

(14) Obrist, D.; Roy, M. E.; Harrison, J.; Kwong, F. C.; Munger, J. W.; Moosmüller, H.; Romero, C.; Sun, S.; Zhou, J.; Commane, R. Previously unaccounted atmospheric mercury deposition in a mid-latitude deciduous forest. *Proc. Natl. Acad. Sci. U.S.A.* **2021**, No. e2105477118.

(15) Stephenson, N. L.; van Mantgem, P. J. Forest turnover rates follow global and regional patterns of productivity. *Ecol. Lett.* **2005**, *8*, 524−531.

(16) Obrist, D.; Pearson, C.; Webster, J.; Kane, T.; Lin, C.-J.; Aiken, G. R.; Alpers, C. N. A synthesis of terrestrial mercury in the western United States: Spatial distribution defined by land cover and plant productivity. *Sci. Total Environ.* **2016**, *568*, 522−535.

(17) Zhao, M.; Running, S. W. Drought-induced reduction in global terrestrial net primary production from 2000 through 2009. *Science* **2010**, *329*, 940−943.

(18) Cleveland, C. C.; Houlton, B. Z.; Smith, W. K.; Marklein, A. R.; Reed, S. C.; Parton, W.; Del Grosso, S. J.; Running, S. W. Patterns of new versus recycled primary production in the terrestrial biosphere. *Proc. Natl. Acad. Sci. U.S.A.* **2013**, *110*, 12733−12737.

(19) Monfreda, C.; Ramankutty, N.; Foley, J. A. Farming the planet: 2. Geographic distribution of crop areas, yields, physiological types, and net primary production in the year 2000. *Global Biogeochem. Cycles* **2008**, *22*, No. GB1022.

(20) Elbert, W.; Weber, B.; Burrows, S.; Steinkamp, J.; Buedel, B.; Andreae, M. O.; Poeschl, U. Contribution of cryptogamic covers to the global cycles of carbon and nitrogen. *Nat. Geosci.* **2012**, *5*, 459−462.

(21) Chave, J.; Andalo, C.; Brown, S.; Cairns, M. A.; Chambers, J. Q.; Eamus, D.; Folster, H.; Fromard, F.; Higuchi, N.; Kira, T.; Lescure, J. P.; Nelson, B. W.; Ogawa, H.; Puig, H.; Riera, B.; Yamakura, T. Tree allometry and improved estimation of carbon stocks and balance in tropical forests. *Oecologia* **2005**, *145*, 87−99.

(22) Pan, S.; Tian, H.; Dangal, S. R. S.; Zhang, C.; Yang, J.; Tao, B.; Ouyang, Z.; Wang, X.; Lu, C.; Ren, W.; Banger, K.; Yang, Q.; Zhang, B.; Li, X. Complex spatiotemporal responses of global terrestrial primary production to climate change and increasing atmospheric CO2 in the 21st Century. *PLoS One* **2014**, *9*, No. e112810.

(23) Chen, S.; Zou, J.; Hu, Z.; Lu, Y. Climate and vegetation drivers of terrestrial carbon fluxes: a global data synthesis. *Adv.Atmos. Sci.* **2019**, *36*, 679−696.

(24) Garkoti, S. C.; Singh, S. Variation in net primary productivity and biomass of forests in the high mountains of Central Himalaya. *J. Veg. Sci.* **1995**, *6*, 23−28.

(25) Lodhiyal, N.; Lodhiyal, L.; Pangtey, Y. Structure and function of Shisham forests in central Himalaya, India: dry matter dynamics. *Ann. Bot.* **2002**, *89*, 41−54.

(26) Fan, H.; Li, Y.; Su, B.; Lin, D.; Liu, C.; Jiang, Z. Allocation pattern of biomass and productivity in the mixed uneven-aged stands of Masson's pine and hardwood species. *Acta Ecol. Sin.* **2006**, *26*, 2463−2473.

(27) Cai, Y.; Zhang, S.; Cai, K.; Huang, F.; Pan, B.; Wang, W. Cd accumulation, biomass and yield of rice are varied with silicon application at different growth phases under high concentration cadmium-contaminated soil. *Chemosphere* **2020**, *242*, No. 125128.

(28) El Mazlouzi, M.; Morel, C.; Robert, T.; Yan, B.; Mollier, A. Phosphorus uptake and partitioning in two durum wheat cultivars with contrasting biomass allocation as affected by different P supply during grain filling. *Plant Soil* **2020**, *449*, 179−192.

(29) Irfan, M.; Aziz, T.; Maqsood, M. A.; Bilal, H. M.; Siddique, K. H. M.; Xu, M. Phosphorus (P) use efficiency in rice is linked to tissue-specific biomass and P allocation patterns. *Sci. Rep.* **2020**, *10*, No. 4278.
(30) Mao, Y.; Li, Y.; Richards, J.; Cai, Y. Investigating uptake and translocation of mercury species by sawgrass (cladium jamaicense) using a stable isotope tracer technique. *Environ. Sci. Technol.* **2013**, *47*, 9678−9684.
(31) Yin, R.; Feng, X.; Meng, B. Stable mercury isotope variation in rice plants (Oryza sativa L.) from the Wanshan mercury mining district, SW China. *Environ. Sci. Technol.* **2013**, *47*, 2238−2245.
(32) Selin, N. E.; Jacob, D. J.; Yantosca, R. M.; Strode, S.; Jaeglé, L.; Sunderland, E. M. Global 3-D land-ocean-atmosphere model for mercury: Present-day versus preindustrial cycles and anthropogenic enrichment factors for deposition. *Global Biogeochem. Cycles* **2008**, *22*, No. GB2011.
(33) Navrátil, T.; Novakova, T.; Roll, M.; Shanley, J. B.; Kopacek, J.; Rohovec, J.; Kana, J.; Cudlin, P. Decreasing litterfall mercury deposition in central European coniferous forests and effects of bark beetle infestation. *Sci. Total Environ.* **2019**, *682*, 213−225.
(34) Zhou, J.; Feng, X. B.; Liu, H. Y.; Zhang, H.; Fu, X. W.; Bao, Z. D.; Wang, X.; Zhang, Y. P. Examination of total mercury inputs by precipitation and litterfall in a remote upland forest of Southwestern China. *Atmos. Environ.* **2013**, *81*, 364−372.
(35) Yuan, W.; Sommar, J.; Lin, C. J.; Wang, X.; Li, K.; Liu, Y.; Zhang, H.; Lu, Z. Y.; Wu, C. S.; Feng, X. B. Stable isotope evidence shows re-emission of elemental mercury vapor occurring after reductive loss from foliage. *Environ. Sci. Technol.* **2019**, *53*, 651−660.
(36) Arnold, J.; Gustin, M. S.; Weisberg, P. J. Evidence for nonstomatal uptake of Hg by aspen and translocation of Hg from foliage to tree rings in Austrian pine. *Environ. Sci. Technol.* **2018**, *52*, 1174−1182.
(37) Peckham, M. A.; Gustin, M. S.; Weisberg, P. J.; Weiss-Penzias, P. Results of a controlled field experiment to assess the use of tree tissue concentrations as bioindicators of air Hg. *Biogeochemistry* **2019**, *142*, 265−279.
(38) Greger, M.; Wang, Y. D.; Neuschutz, C. Absence of Hg transpiration by shoot after Hg uptake by roots of six terrestrial plant species. *Environ. Pollut.* **2005**, *134*, 201−208.
(39) Clackett, S. P.; Porter, T. J.; Lehnherr, I. 400-year record of atmospheric mercury from tree-rings in Northwestern Canada. *Environ. Sci. Technol.* **2018**, *52*, 9625−9633.
(40) Hojdová, M.; Navratil, T.; Rohovec, J.; Zak, K.; Vanek, A.; Chrastny, V.; Bace, R.; Svoboda, M. Changes in Mercury Deposition in a Mining and Smelting Region as Recorded in Tree Rings. *Water, Air, Soil Pollut.* **2011**, *216*, 73−82.
(41) Jung, R.; Ahn, Y. S. Distribution of mercury concentrations in tree rings and surface soils adjacent to a phosphate fertilizer plant in southern Korea. *Bull. Environ. Contam. Toxicol.* **2017**, *99*, 253−257.
(42) Kang, H. H.; Liu, X. H.; Guo, J. M.; Wang, B.; Xu, G. B.; Wu, G. J.; Kang, S. C.; Huang, J. Characterization of mercury concentration from soils to needle and tree rings of Schrenk spruce (Picea schrenkiana) of the middle Tianshan Mountains, northwestern China. *Ecol. Indic.* **2019**, *104*, 24−31.
(43) Navrátil, T.; Novakova, T.; Shanley, J. B.; Rohovec, J.; Matouskova, S.; Vankova, M.; Norton, S. A. Larch Tree Rings as a Tool for Reconstructing 20th Century Central European Atmospheric Mercury Trends. *Environ. Sci. Technol.* **2018**, *52*, 11060−11068.
(44) Navrátil, T.; Simecek, M.; Shanley, J. B.; Rohovec, J.; Hojdova, M.; Houska, J. The history of mercury pollution near the Spolana chlor-alkali plant (Neratovice, Czech Republic) as recorded by Scots pine tree rings and other bioindicators. *Sci. Total Environ.* **2017**, *586*, 1182−1192.
(45) Schneider, L.; Allen, K.; Walker, M.; Morgan, C.; Haberle, S. Using Tree Rings to Track Atmospheric Mercury Pollution in Australia: The Legacy of Mining in Tasmania. *Environ. Sci. Technol.* **2019**, *53*, 5697−5706.
(46) Wright, G.; Woodward, C.; Peri, L.; Weisberg, P. J.; Gustin, M. S. Application of tree rings dendrochemistry for detecting historical trends in air Hg concentrations across multiple scales. *Biogeochemistry* **2014**, *120*, 149−162.
(47) Zhou, J.; Wang, Z. W.; Zhang, X. S.; Gao, Y. Mercury concentrations and pools in four adjacent coniferous and deciduous upland forests in Beijing, China. *J. Geophys. Res.: Biogeosci.* **2017**, *122*, 1260−1274.
(48) Huhn, G.; Schulz, H.; Stark, H. J.; Tolle, R.; Schuurmann, G. Evaluation of regional heavy-metal deposition by multivariate-analysis of element contents in pine tree barks. *Water, Air, Soil Pollut.* **1995**, *84*, 367−383.
(49) Chowdhury, R.; Favas, P. J. C.; Jonathan, M. P.; Venkatachalam, P.; Raja, P.; Sarkar, S. K. Bioremoval of trace metals from rhizosediment by mangrove plants in Indian Sundarban Wetland. *Mar. Pollut. Bull.* **2017**, *124*, 1078−1088.
(50) Chiarantini, L.; Rimondi, V.; Benvenuti, M.; Beutel, M. W.; Costagliola, P.; Gonnelli, C.; Lattanzi, P.; Paolieri, M. Black pine (Pinus nigra) barks as biomonitors of airborne mercury pollution. *Sci. Total Environ.* **2016**, *569*−*570*, 105−113.
(51) Serbula, S. M.; Miljkovic, D. D.; Kovacevic, R. M.; Ilic, A. A. Assessment of airborne heavy metal pollution using plant parts and topsoil. *Ecotoxicol. Environ. Saf.* **2012**, *76*, 209−214.
(52) Huang, S.; Jiang, R.; Song, Q.; Zhang, Y.; Huang, Q.; Su, B.; Chen, Y.; Huo, Y.; Lin, H. Study of mercury transport and transformation in mangrove forests using stable mercury isotopes. *Sci. Total Environ.* **2020**, *704*, No. 135928.
(53) Woś, B.; Sroka, K.; Jozefowska, A.; Pietrzykowski, M. Mercury concentration in technosols and alder tissue from a plantation on a combustion waste disposal site. *Water, Air, Soil Pollut.* **2019**, *230*, 259.
(54) Cui, L. W.; Feng, X. B.; Lin, C. J.; Wang, X. M.; Meng, B.; Wang, X.; Wang, H. Accumulation and translocation of (198)Hg in four crop species. *Environ. Toxicol. Chem.* **2014**, *33*, 334−340.
(55) Niu, Z. C.; Zhang, X. S.; Wang, Z. W.; Ci, Z. J. Field controlled experiments of mercury accumulation in crops from air and soil. *Environ. Pollut.* **2011**, *159*, 2684−2689.
(56) Witt, E. L.; Kolka, R. K.; Nater, E. A.; Wickman, T. R. Influence of the forest canopy on total and methyl mercury deposition in the boreal forest. *Water, Air, Soil Pollut.* **2009**, *199*, 3−11.
(57) Fu, X.; Zhu, W.; Zhang, H.; Sommar, J.; Yu, B.; Yang, X.; Wang, X.; Lin, C.-J.; Feng, X. Depletion of atmospheric gaseous elemental mercury by plant uptake at Mt. Changbai, Northeast China. *Atmos. Chem. Phys.* **2016**, *16*, 12861−12873.
(58) Zheng, W.; Obrist, D.; Weis, D.; Bergquist, B. A. Mercury isotope compositions across North American forests. *Global Biogeochem. Cycles* **2016**, *30*, 1475−1492.
(59) Zhou, J.; Du, B. Y.; Shang, L. H.; Wang, Z. W.; Cui, H. B.; Fan, X. J.; Zhou, J. Mercury fluxes, budgets, and pools in forest ecosystems of China: A review. *Crit. Rev. Environ. Sci. Technol.* **2020**, *50*, 1411−1450.
(60) Bieser, J.; Slemr, F.; Ambrose, J.; Brenninkmeijer, C.; Brooks, S.; Dastoor, A.; DeSimone, F.; Ebinghaus, R.; Gencarelli, C. N.; Geyer, B.; Gratz, L. E.; Hedgecock, I. M.; Jaffe, D.; Kelley, P.; Lin, C. J.; Jaegle, L.; Matthias, V.; Ryjkov, A.; Selin, N. E.; Song, S.; Travnikov, O.; Weigelt, A.; Luke, W.; Ren, X.; Zahn, A.; Yang, X.; Zhu, Y.; Pirrone, N. Multi-model study of mercury dispersion in the atmosphere: vertical and interhemispheric distribution of mercury species. *Atmos. Chem. Phys.* **2017**, *17*, 6925−6955.
(61) Agnan, Y.; Le Dantec, T.; Moore, C. W.; Edwards, G. C.; Obrist, D. New constraints on terrestrial surface atmosphere fluxes of gaseous elemental mercury using a global database. *Environ. Sci. Technol.* **2016**, *50*, 507−524.

https://doi.org/10.1021/acs.est.1c03530
Environ. Sci. Technol. 2021, 55, 14245−14257